ACS OMEGA

http://pubs.acs.org/journal/acsodf

Article

Optimization of a Thermal Cracking Reactor Using Genetic Algorithm and Water Cycle Algorithm

Peyman Roudgar Saffari, Hesamoddin Salarian, Ali lohrasbi, Gholamreza Salehi,* and Mohammad Hasan Khoshgoftar Manesh

Cite This: *ACS Omega* 2022, 7, 12493−12508

Read Online

ACCESS | Metrics & More | Article Recommendations

ABSTRACT: With the global production of 150 million tons in 2016, ethylene is one of the most significant building blocks in today's chemical industry. Most ethylene is now produced in cracking furnaces by thermal cracking of fossil feedstocks with steam. This process consumes around 8% of the main energy used in the petrochemical industry, making it the single most energy-intensive process in the chemical industry. This paper studies a tubular thermal cracking reactor fed by propane and the molecular mechanism of the reaction within the reactor. After developing the reaction model, the existing issues, such as the reaction, flow, momentum, and energy, were resolved by applying heat to the outer tube wall. After solving the entropy generation equations, the entropy generation ratio of the sources was evaluated. The temperature of the tube/reactor was tuned following the reference results, and processes were replicated for different states. The verification of the modeling and simulation results was compared with the industrial case. The Genetic Programming (GP) machine learning approach was employed to generate objective functions based on key decision variables to reduce the computational time of the optimization algorithm. For the first time, this study has proposed a systematic approach for optimizing a thermal cracking reactor based on a combination of Genetic Programming (GP), Water Cycle Algorithm (WCA), and Genetic Algorithm (GA). In this regard, multiobjective optimization was performed based on the maximization of the products and entropy generation with the generation of GP objective functions. The key decision variables in this study included inlet gas temperature, inlet gas pressure, air mass flow rate, and wall temperature. The results showed that the weighted percentage of products after optimization increased to 61.13% and the entropy production rate of the system decreased to 899.80 J/s, displaying an improvement of 0.85 and 16.51% compared with the base case, respectively, with the multiobjective GA algorithm. In addition, by applying the multiobjective WCA, the weighted percentage of products increased to 61.81%. The entropy production rate of the system decreased to 882.72 J/s. So, an improvement of 1.97% in weights of products and an improvement of 18.77% in entropy generation have been achieved compared with the base case.

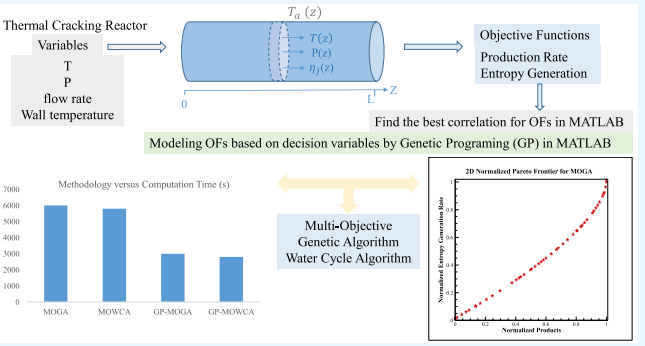

1. INTRODUCTION

The thermal cracking of hydrocarbons is the most common form of olefin production. The thermal cracking of propane is conducted using a radical mechanism that is highly studied and researched by Zhou et al.,[1] who conducted an entropy generation minimization in a solid reactor based on construction theory; their model consisted of 10 reactions. The molecular model of reactions performs quickly and is broadly applied in ref 2 for the simulation of propane thermal cracking. An industrial cracker was simulated in ref 2 using the presented scheme. They developed a molecular model for nine reactions with nine components. Masoumi et al.[3] studied the thermal cracking furnace and monitored its dynamic behavior. To this end, they built a pilot plant controlled by a computer system. The steady-state model had one dimension, 543 reactions, and 90 elements. They intended to enhance the steady-state to gain maximum advantage. Gao et al.[2] modeled the tubular reactor in a naphtha cracking furnace to optimize it using the HYSYS software package. Their method also enhanced the operation profitability considerably. Process assessment was conducted under steady-state circumstances. However, the real-world coke formation is time-dependent, affecting the efficiency; they did not consider coke thickness in the heat transfer coefficient.

Received: August 18, 2021
Accepted: March 16, 2022
Published: April 2, 2022

https://doi.org/10.1021/acsomega.1c04345
ACS Omega 2022, 7, 12493−12508

Ghasemi et al.[4] used a 3D model and computational fluid dynamics to study the ethylene furnace. The temperatures of the tube skin and heat flux profiles were measured by solving the mass, momentum, and energy equations corresponding to furnaces in Ansys Fluent. The results indicated that by increasing the fuel rate, outlet propylene yield decreased, while process gas temperature, pressure drop, propane conversion, and ethylene yield were increased along the reactor tube. In addition, increasing reactor feed flow rate increased the desired product yields, despite the reduction in the coil outlet temperature of the reactor.

Ghasghaee and Karimzadeh[5] attempted to use a dynamic model to explain why cracks show an unsteady-state behavior during their start-up in furnaces. Their mathematical model, the convection model, comprised four sub-models: cylindrical coil, combustion chamber, and shell and tube. They captured a two-dimensional zone to predict the factors at a start-up run using these four sub-models. Zheng et al.[6] calculated the heat flow and temperature distribution using CFD 3D modeling in the thermal cracking reactor and furnace and compared the results using spectrometry. Barazandeh et al.[7] investigated a liquid furnace using a 1-D mathematical model to analyze the furnace temperature profile and how it affects the feed-to-product conversion percentage.

Heat transfer and its entropy generation have gained vast attention in the research community. Entropy induction limitations are variable in a closed system concerning the applied law of heat transfer. Closed systems are important since they are simple, depict the main principles, and investigate the process. Nummedal and Kjelstrup[8] employed the thermodynamic equipartition of force (EOF) theory to study entropy generation in a heat exchanger. They showed that the optimal operation of one heat exchanger was the operation that was known for long from experience, namely the one given by specific counter-current flows. The result was aligned with the EOF principle.

Sauar et al.[9] and Kjelstrup and Island[10] also used the EOF principle for a chemical reactor. The EOF theory holds that the entropy generated by a system is minimum when the thermodynamic forces are constant in terms of time or space. This theory applies to processes in which independent events do not communicate. However, the theory of EOF fails to justify the comparison between the real minimum entropy generated in a chemical reactor and the law of mass conservation issues in the distillation tower.[11]

Numerous research studies have addressed the entropy generation problem using the governing equations,[12−14] Nummedal and Kjelstrup[8] examined the generation of entropy and the process of heat transfer using EOF and EOEP methods. Sauar et al.[9] and Kjelstrup et al.[10] applied EOF theory in chemical reactors as an appropriate approach for analyzing them. Wilhelmsen et al. investigated the energy-efficient reactor design simplified with entropy analysis.[15] The mentioned studies also model a set of guidelines to achieve reactor design with energy efficiency, which can be applied once the best available heat transfer coefficients have been reached. The optimal design was related to the heat transfer coefficient relative size across the wall of the tubular reactor and heat transfer coefficients in heat exchangers.

The main drawbacks are the nonlinear relations of the flow and force concerned with the chemical reactions. Wilhelmsen et al.[16] studied hydrogen producer steam reformers extensively.

Johannessen and Kjelstrup[16] minimized entropy generation in the reactor using optimal control theory. They considered temperature a control variable and used governing equations of the plug flow reaction and SO_2 oxidation to show a way to minimize the entropy generation rate in plug flow reactors by optimal control theory. It is demonstrated that decreasing the entropy generation rate up to 25% can be obtained by changing the reactor length and controlling the utility. A hypothesis was proposed that a reactor with high energy efficiency had relatively long sections with constant entropy generation rate and driving forces.

Kingston and Razzitte[17] investigated the unique kinds of continuously stirred tank reactors (CSTRs) and plug flow reactors (PFRs). They also verified the temperature and pressure and gave a graphical picture of entropy generation in chemical reactions to constant volume, allowing access to different options efficiently. Also, they indicated that by dividing a reactor into two smaller ones, with different operating temperatures, the entropy generation decreased, going as near as 48% less in the case of a CSTR and PFR in series, and achieving 58% with two CSTR.

Chen et al.[18] produced light olefins using CO_2 hydrogenation to minimize entropy production. Røsjorde et al.[19] attempted to minimize entropy production in propane dehydrogenation using different tower condenser reactor and exchanger components. The structural theory to model and minimize entropy generation has been used. Abdous et al.[20] analyzed the same problem in helically coiled tubes under flow boiling conditions under a constant heat flux. Kurnia et al.[21] applied this analysis to various cross-sections.

Vandewalle et al.[22] used computational fluid dynamic (CFD) fouling in steam cracking reactors and developed a 3D algorithm to simulate coke formation in steam cracking reactors. They examined coke layer growth to analyze a reactor's run length and determined that the ribbed reactor design had the most extended run length.

Mu and Gu[23] studied the optimal modeling of thermal cracking furnaces based on the enriched Kumar model by considering free-radical reactions. An improved search engine algorithm (IPR) was developed to compute the importance of substances in the Kumar model for efficient model selection. The proposed model indicated that the new model achieved a mean relative error (MRE) of less than 0.1% compared to 5% in the Kumar model. The proposed model could be applied to modeling extensive feedstocks with high accuracy.

Zhou et al.[24] optimized the ethane thermal cracking furnace via the coupling of the reaction network. The residence time related to the minimum by-product was determined to be 0.4 s, and its by-product was 4.3% less than that at the initial residence time (0.3 s).

Gold yttrium oxide nanorods for oxidative catalytic cracking of *n*-propane to light olefins have been studied by Narasimharao and Alshehri.[25] Gold nanoparticles loading has affected the activity of oxidative catalytic cracking. In addition, simple Au-O-Y species and Lewis acid sites are provided for the activity.

Ebrahimian et al.[26] proposed an innovative reactor concept for thermal coupling of naphtha reformation with propane ammoxidation. The production of aromatics, hydrogen, and acrylonitrile have been considered. The evaluation of the thermally coupled reactors with the conventional reactors has been performed—eliminating traditional furnaces in naphtha reforming.

https://doi.org/10.1021/acsomega.1c04345
ACS Omega 2022, 7, 12493−12508

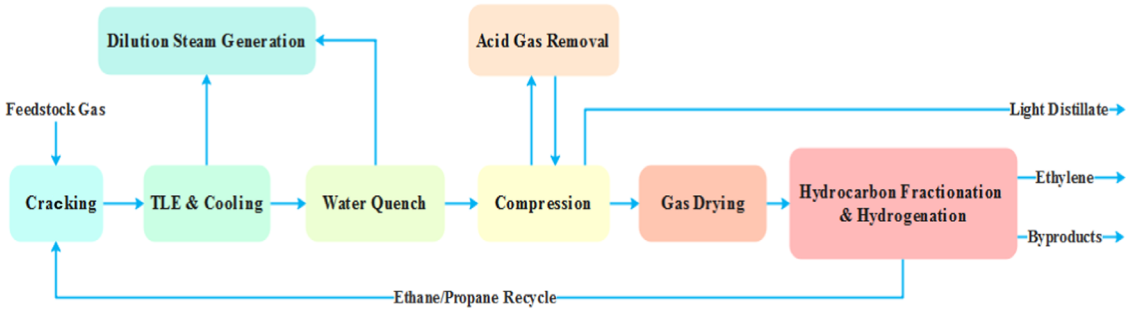

Figure 1. Hydrocarbon thermal cracking process.[34]

A comprehensive investigation on hydrogen production through propane steam reforming inside a reactor has been performed by Barnoon et al.[27] The results demonstrate that the hydrogen generation yield can change from 77.5 to 92.2%. The reaction rate can be varied by the velocity and temperatures of the hot gases. Also, for T = 900 K, full propane used is obtained at the reformer outlet.

Simulation and dynamic optimization to find optimum operational parameters of the industrial tubular reactor for propane cracking have been investigated by Berreni and Wang.[28] This work was performed in gPROMS. The steady-state and dynamic optimizations were respectively performed. The results show that dynamic optimization can improve the net profit by 10.6% rather than the base case. In addition, the computation demand by dynamic optimization was much wider and higher than the steady-state optimization.

A coupled CFD simulation method for investigating the pyrolysis process in industrial naphtha thermal cracking furnaces has been performed by Rezaeimanesh et al.[29] A typical $k-\varepsilon$ turbulence model is combined with the molecular kinetic response for cracking, a thorough combustion model, and radiative properties in this full CFD model. The simulation results corresponded well with industrial data acquired from a mega olefin plant of a petrochemical complex in terms of temperature, product yield, and especially propylene-to-ethylene ratio (P/E). The difference between P/E resulting from industrial data was less than 2%.

From the standpoint of intelligent manufacturing, knowledge expression, numerical modeling, and optimization application of ethylene thermal cracking have been investigated by Zhang et al.[30] This study presented a summary of advances and contributions to PSE-assisted thermal cracking production; it introduces the frameworks, methodologies, and algorithms suggested over the last 10 years; and it explores the benefits, limitations, and industrial applications.

Yuan et al.[31] performed advanced exergy analysis to assess the energy-saving potential of industrial ethylene cracking furnaces. Inside the furnace, a simulation is run that considers the interactions of three different components. The highest exergy degradation occurs during the combustion process in the radiation section. High avoidable exergy destruction in tube reactors and combustion processes have been found.

Monitoring of combustion in an industrial cracking furnace using a combination of CFD and visual techniques has been investigated by Rebordinos et al.[32] A new methodology based on CFD calculations of OH− and CH− radicals via decreased chemical kinetics and industrial-scale experimental validation using flame spectroscopic measurements and UV CCD cameras have been developed to monitor burner efficiency. Second, NOx emissions have been simulated using the standard approach of reduced chemistry and post-processing over the CFD fields, proving that realistic predictions can be made in this setting using plant data at the stack.

For an ethylene-cracking furnace with many faults and exceptional operation conditions, a two-level completely energy-efficient quantitative diagnosis method was developed by Meng et al.[33] The goal of energy efficiency diagnosis was to determine the severity and root causes of various types of inefficiency. More accurate findings are obtained when a mechanism and a data-driven multiple benchmark criteria are coupled.

Saffari et al.[34] assessed the entropy generation in a thermal cracking reactor. The results indicated for two states that the three factors were in the order of chemical reactions, heat transfer, and pressure loss in terms of their contribution to entropy generation. The variation of feed temperature did not affect the entropy generated by the chemical reactions. However, the entropy generation in the reactor with optimum wall temperature was the lowest. Also, entropy was higher at the inlet of the reactor when the wall had an optimal temperature.

Previous studies rely on basic principles of flow, chemical reactions, and fundamental energy equations, which do not involve minimization of entropy generation and its adequation for the process. A review of previous research shows no investigation of optimizing thermal cracking reactors by addressing maximum productivity and minimum entropy generation. In addition, no systematic approach has been adopted for the multiobjective optimization of thermal cracking reactors. The innovation of this study is that it has, for the first time, addressed the maximization of productivity, and minimization of entropy generation have been considered simultaneously. In this regard, the second law of thermodynamics and the entropy production rate were employed. Considering entropy generation sources, the basic factors, and mitigating its generation, enhance the process that may lead to a better economization. Also, a systematic approach was adopted based on the genetic programming (GP) technique for the multiobjective optimization of thermal cracking reactors based on key parameters based on minimizing entropy generation and maximizing products. The GP technique reduced the run time and obtained high convergence to two objectives optimization.

2. THERMAL CRACKING PROCESS

Lighter product yield when the hydrocarbon feed flows at a high speed within a thermal cracking reactor at 800−900 °C with dilution steam. The reactor outlets are mainly ethylene and propylene, as well as olefin, butadiene, and aromatics. The outlet reactor products rapidly cooled down to 300 °C to prevent unwanted reactions. High-pressure steam was generated using

https://doi.org/10.1021/acsomega.1c04345
ACS Omega 2022, 7, 12493−12508

Table 1. Study Reactor's Specifications[28]

parameters/variable	value
length of the coil in the radiant section	95 [m]
length of the straight portion of the coil	8.85 [m]
length of the bends	0.554 [m]
the radius of the bends	0.178 [m]
tube internal diameter	0.108 [m]
wall thickness	0.008 [m]
total feed per coil	0.7635 [kg/s]
steam dilution rate	0.4 [kg steam/kg propane]
inlet pressure	3 [bar]
inlet temperature	873.15 [K]

the resulting energy. Then water and oil were injected to reduce the temperature of the products to virtually room temperature and split up the heavy elements. The pressure of the outlets was then increased to 35 bar. They were sent for fractionation to split up the primary products.[35]

Figure 1 is a representation of the process. Thermal cracking reactors are influenced by various performance factors, such as feed composition and feed quantity, reactor pressure and temperature, the amount of the dilution steam, and reactor residence time. The coke precipitate remains on the reactor walls and impairs the furnace's performance. Monitoring and controlling the optimum factors and parameters enhances the operation and improves the furnace performance.

The reactor resides on the thermal cracking furnace that provides the required heat for the reactions. The inside temperature of the reactor is an essential parameter in thermal cracking reactions due to their endothermic characteristic. Heat flux increasing in the outgoing reactor surface to the highest possible allowed level may expand the amounts of undesirable products such as coke. Therefore, the reactor temperature should be regulated to increase the desired products instead of undesired products. The temperature was increased due to the resident materials in the outlet of the reactor. Nevertheless, the flow should get consistent heat during its process inside the reactor axle. Overheating leads to hot spots and generates local coke.[28]

The position of the reactors in thermal cracking furnaces is different. They may be established either in parallel or vertical to the floor regarding the furnace type. Normally, variable-diameter reactors are used as an option for liquid feeds. However, fixed-diameter reactors are used for gassy feeds. The number of reactor paths inside the furnace may vary based on the available technical knowledge.

2.1. Reactor Specifications. The employed reactor is the same as in ref 28 fed by pure propane. Table 1 illustrates the required details.

3. MATHEMATICAL MODEL OF THE THERMAL CRACKING REACTOR

Berreni and Wang prepared an accurate mathematical model of an industrial thermal cracking reactor. Accordingly, the mathematical models were extracted from ref 28. For simplicity, a simple scheme is presented in Figure 2. In addition, other relevant equations were extracted from ref 36.

3.1. Mass Balance Equation. The following equation captures the mass balance for the *j*th component of the reaction mix along the d*z* length of the reactor

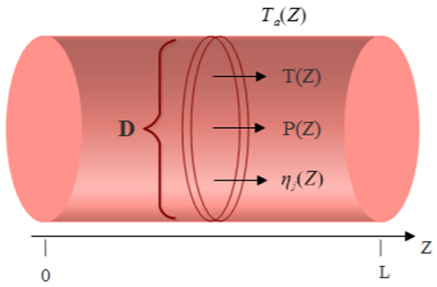

Figure 2. Schematic illustration of a thermal cracking reactor.[34]

$$\frac{dF_j}{dz} = R_j \frac{\pi d_t^2}{4} = \left(\sum_i \alpha_{ij} r_i\right) \frac{\pi d_t^2}{4} \tag{1}$$

where r_i represents the speed of the *i*th reaction. The following equation captures r_i:

$$r_i = K_i \prod c_j^{|\alpha_{ij}|} \tag{2}$$

The molar flow/pressure rate should be considered to apply the speed law. Assuming all the gases as ideal, the general law of gas indicates

$$c_j = \frac{P_j}{RT} = \frac{y_j P_t}{RT} \tag{3}$$

Replacing y_j (the molar ratio) with its equivalent, $y_j = \frac{F_j}{F_t}$, leads to

$$c_j = \frac{F_j P_t}{F_T RT} \tag{4}$$

3.2. Energy Balance Equation. Equation 5 captures the energy balance along the reactor[28]

$$\frac{dT}{dz} = \frac{1}{\sum_j F_j C_{pj}} \left(J_q(z) \pi d_t + \frac{\pi d_t^2}{4} \sum_i r_i (-\Delta H_i) \right) \tag{5}$$

3.3. Momentum Balance. Equation 6 captures the pressure

$$\frac{-dP_t}{dz} = \alpha \left[\frac{2f}{d_t} + \frac{\xi}{\pi r_b} \right] \rho_g u^2 + \alpha \rho_g u \frac{du}{dz} \tag{6}$$

The first term on the right-hand side is friction-induced pressure loss. The second term captures the pressure loss induced by momentum change. Regarding the continuity law and the assumption of the gas ideality, the following equations are derived[28]

$$G = pu = \text{const} \tag{7}$$

$$\rho = \frac{M_m P_t}{RT} \tag{8}$$

$$u = \frac{G}{M_m} \cdot \frac{RT}{P_t} \tag{9}$$

$$\frac{du}{dz} = \frac{GR}{P_t} \left[T \frac{d(1/M_m)}{dz} + \frac{1}{M_m} \cdot \frac{dT}{dz} \right] - \frac{GRT}{M_m P_t^2} \cdot \frac{dP}{dz} \tag{10}$$

Substituting the equations gives

https://doi.org/10.1021/acsomega.1c04345
ACS Omega 2022, 7, 12493−12508

Table 2. Reactions Involved in the Thermal Cracking of Propane[37]

no	reaction	$A(1/S$, m^3/kmol·S or kgS/mol·m)	E (kJ/mol)	ΔH (kJ/mol, @298 K)
1	$C_3H_8 \leftrightarrow C_2H_4 + H_4$	4.692×10^{10}	211.7	82.66
2	$C_3H_8 \leftrightarrow C_3H_6 + H_2$	5.888×10^{10}	214.6	124.68
3	$C_3H_8 + C_2H_4 \rightarrow C_2H_6 + C_3H_6$	2.536×10^{13}	241.7	−11.64
4	$2C_3H_6 \rightarrow 3C_2H_4$	1.514×10^{11}	233.5	117.5
5	$2C_3H_6 \rightarrow 0.5C_6 + 3CH_4$	1.423×10^{9}	190.4	−14.48
6	$C_3H_6 \leftrightarrow C_2H_2 + CH_4$	3.794×10^{11}	248.5	96.4
7	$C_3H_6 + C_2H_6 \rightarrow C_4H_8 + CH_4$	5.553×10^{14}	251.1	−11.24
8	$C_2H_6 \leftrightarrow C_2H_4 + H_2$	4.652×10^{13}	272.8	136.32
9	$C_2H_4 + C_2H_2 \rightarrow C_4H_6$	1.026×10^{12}	172.6	−133.42
10	$C_4H_8 \rightarrow C_6$	6.92×10^{7}	143.6	83.42

$$\frac{dP_t}{dz} = \frac{\frac{d(1/M_m)}{dz} + \frac{1}{M_m}\left(\frac{1}{T}\frac{dT}{dz} + Fr\right)}{\frac{1}{M_m P_t} - \frac{P_t}{\alpha G^2 RT}} \tag{11}$$

The friction function for the direct section of the tube is defined as[28]

$$Fr = \frac{2f}{d_t} = 0.092Re^{-0.2/d_t} \tag{12}$$

The bends equations are defined as

$$Fr = 0.092Re^{-0.2/d_t} + \zeta / \pi R_b \tag{13}$$

$$\zeta = \left(0.7 + \frac{\Lambda}{90^\circ} \times 0.35\right)\xi \tag{14}$$

$$\xi = 0.051 + 0.19\frac{d_t}{R_b} \tag{15}$$

The following equation may be replaced in the pressure equation[28]

$$\frac{d(1/M_m)}{dz} = \frac{d}{dz}\left(\frac{\sum_j F_j}{G\Omega}\right) = \frac{\sum_j \frac{dF_j}{dz}}{G\Omega} \tag{16}$$

3.4. Calculation of Convection Heat Transfer in Reactor Outlets. The following equations illustrate the calculation of convection heat transfer[28]

$$q = hA(T_w - T_b)_{av} \tag{17}$$

$$T_b = \frac{\int_0^R l2\pi dr UC_p T}{\int_0^R l2\pi dr UC_p} \tag{18}$$

$$q = mC_p(T_{bo} - T_{bi}) \tag{19}$$

$$Nu = 0.023Re_D^{0.8}Pr^n \tag{20}$$

where $n = 0.4$ outlet heating, $T_w > T_b$, $L/D > 60$, $6000 < Re_D < 10^7$.

3.5. Entropy Generation in the Thermal Cracking Reactor. The reactor is supposed to function in a stable or steady state. Therefore the entropy balance of the system includes three additional terms. Heat transfer induces two additional entropy factors to the system. So, the following equation captures the amount of entropy generation[16]

$$\left(\frac{ds}{dt}\right)_{irr} = s_{out} - s_{in} + \Delta s_u \tag{21}$$

For a small element dz, we have $\Delta S_u = -\pi D J_q(z)/Ta(z)dz$. The following illustrates the final entropy generation equation by entropy balance[16]

$$\left(\frac{ds}{dt}\right)_{irr} = s_{out} - s_{in} - \pi d_t \int_0^L \frac{J_q(z)}{T_a(z)}dz \tag{22}$$

$$\left(\frac{ds}{dt}\right)_{irr} = \int_0^L \left(\frac{ds}{dz} - \pi d_t \frac{J_q(z)}{T_a}\right)dz \tag{23}$$

$$\sigma = \frac{ds}{dz} - \pi d_t \frac{J_q(z)}{T_a} \tag{24}$$

Using

$$v = \frac{(F_T/\Omega)RT}{P} \tag{25}$$

$$\Delta\left(\frac{1}{T}\right) = \frac{1}{T(z)} - \frac{1}{T_a(z)} \tag{26}$$

the local entropy generation becomes[39]

$$\sigma = \pi d_t J_q(z)\Delta\left(\frac{1}{T}\right) + \Omega v\left(-\frac{1}{T}\frac{dP}{dz}\right) + \frac{\pi d_t^2}{4}\sum_i r_i\left(\frac{-\Delta G_i}{T}\right) \tag{27}$$

Equation 27 shows three facts responsible for entropy in a chemical reactor: the heat transfer to the reactor wall, chemical reactions, and pressure loss. The terms of the above equation result from multiplying thermodynamic flux and its relevant force. The first term includes the multiplication of heat flux $J_q(z)$ and its thermodynamic force $\Delta(1/T)$, the second term includes the multiplication of velocity flux and its thermodynamic force $\left(-\frac{1}{T}\frac{dP}{dz}\right)$, and the last term includes the multiplication of the velocity flux of the reaction r_i and its thermodynamic force $\left(\frac{-\Delta G_i}{T}\right)$.

Integrating σ over the reactor length captures the amount of entropy generation as in the following equation

$$\left(\frac{ds}{dt}\right)_{irr} = \int_0^L \sigma dz \tag{28}$$

3.6. Kinetic Model Selected for the Research. The molecular mechanism used in this work has been proposed by the authors in ref 37. Propane and water steam were fed into the reactor; they were converted into 12 components throughout 11 reactions. Water steam reactions with other components were

https://doi.org/10.1021/acsomega.1c04345
ACS Omega 2022, 7, 12493−12508

Data: Objective function $Products(x), S_{g_{total}}(x)$

Constraints: c(1) : c(5)

Results: Near-optimal solution x

1. Create initial random population $g(t)$
2. **While** *stopping criteria is not met,* **do**
   3. Read (current-generation $g(t)$)
   4. Selection (current-generation $S(t)$)
   5. Crossover (Offspring $C(s)$)
   6. Mutation (Offspring $M(s)$)
   7. Evaluate fitness (Offspring $F(s)$)
   8. Elitism (current-generation $g(t+1)$)

end

Figure 3. Pseudocode for the MOGA algorithm.

ignored. Table 2 shows these reactions, the activation energy, and the Arrhenius equation factor. Coke formation is ignored in this study. The following equation captures the velocity specific to the reaction K, which is a function of temperature[37]

$$K = A\exp(-E / RT) \tag{29}$$

where A is the exponential function coefficient or frequency factor, E is the activation energy (J/mol or cal/mol), R is the ideal gas constant, and T shows the absolute temperature (K).

3.7. Assumptions and Problem-Solving Procedures.

The reactor model is addressed in this section. The pressure, temperature, and weight percent data related to the components and reactor length are used to assess entropy. The reactor simulation assumptions are as follows:

- It is assumed that the internal flow of the reactor is plug flow; because the velocity of the gas is high and the reactor diameter is negligible compared to its length; thus, the axial dispersion of the reactor is ignorable. This assumption is valid based on ref 28.
- Coke deposition is ignored, and the reactor is assumed to be steady-state.

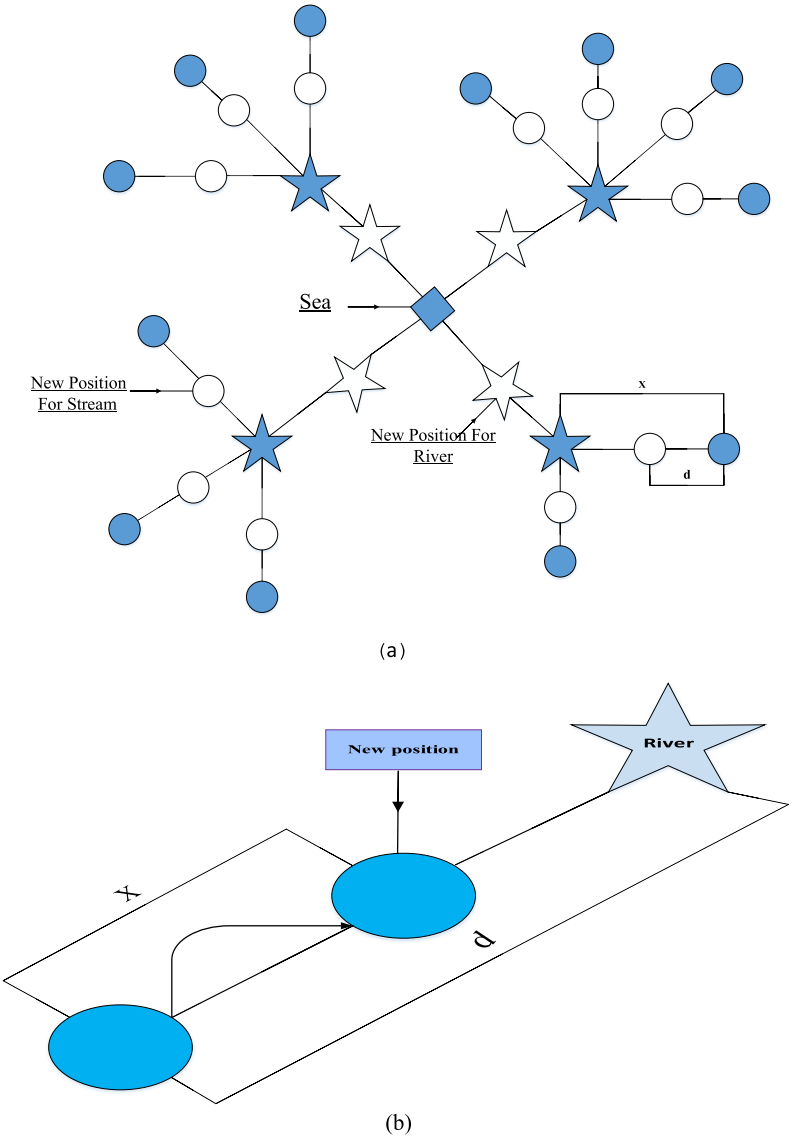

Figure 4. (a) Schematic description of the stream's flow to a specific river and (b) schematic of the WCA optimization process.[39]

https://doi.org/10.1021/acsomega.1c04345
ACS Omega 2022, 7, 12493−12508

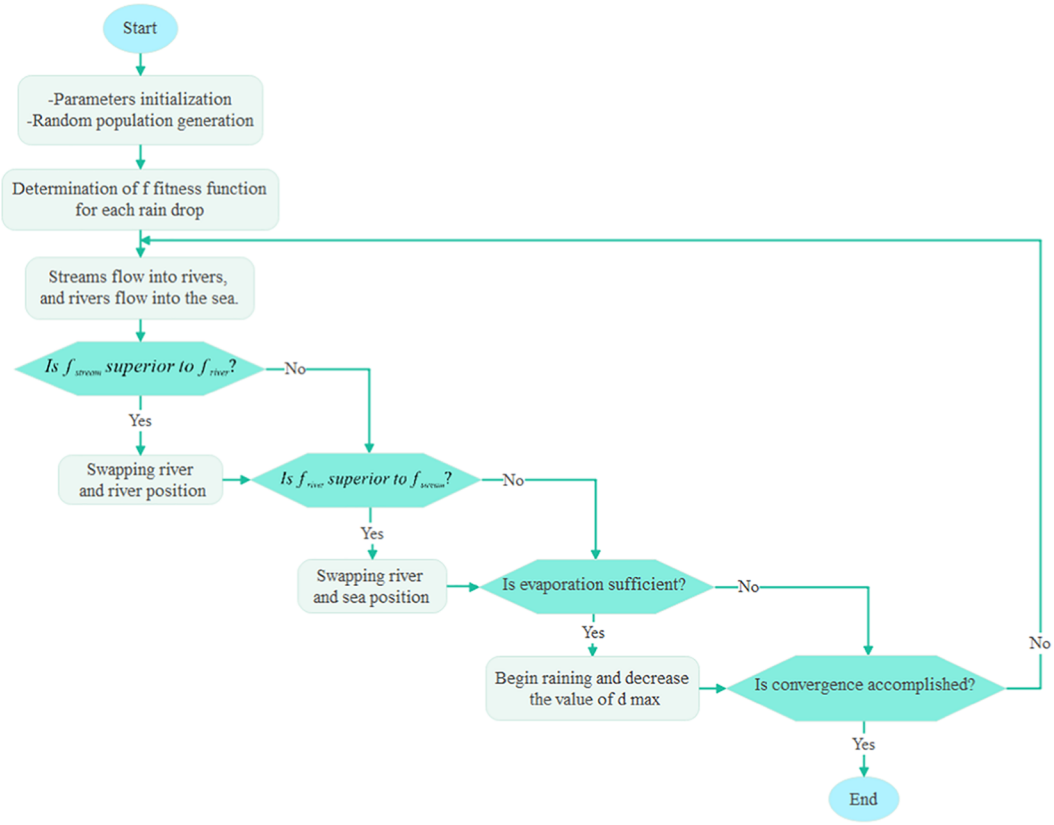

Figure 5. Flowchart of the water cycle algorithm.

Table 3. Key Decision Variables and Constraints

decision variables	unit	lower limit	upper limit
inlet gas temperature	K	700	1000
inlet gas pressure	bar	2	6
inlet mass flow rate of gases	g/s	500	900
wall temperature	K	950	1300

- The internal space of the reactor is assumed to be filled only with the combination of gas and steam.
- The reactions initiate from the input and terminate in the reactor's output.
- The input/output hydrodynamic and thermal zone effects are not considered.
- The concentrations are captured using the law of ideal gas.

The relevant equations, i.e., energy, molar, and momentum balance, need to be solved simultaneously.

After performing 10 chemical reactions, the feed and pure propane resulted in 10 individual components. Table 2 demonstrates the results. A differential equation is derivable for the components. The molar balance questions are initially equal to zero, except for propane, whose value is given in Table 2.

The input feed temperature is required to solve the energy equation, which is a function of the temperature of the outer surface, and its profile is provided based on the length of the reference reactor.[28] Finally, the initial input pressure for the pressure loss equation is known. There are 12 differential equations whose initial conditions are known. They were solved using the MATLAB software package, using the *ode*15*s* function, solving complicated differential equations using the GEAR method. Now that all required factors are known, the integral generated in the reactor may be calculated.

4. OPTIMIZATION

In this study, two optimization algorithms were used: the multiobjective genetic algorithm (MOGA), a well-known and efficient method for multiobjective optimization, and the multiobjective water cycle algorithm (MOWCA), which is an attractive, recent, and simple concept.

4.1. MOGA. While GA considered problems with one objective function, MOGAs can overcome this limitation and simultaneously consider two or more objectives. In many industrial problems, objectives under consideration conflict with each other, and optimizing a particular solution related to a single-objective can result in unacceptable results dealing with the other objectives. A reasonable solution to a multiobjective problem is to investigate a set of solutions, each of which satisfies the objectives at an acceptable level without being dominated by any other solution.[38] Equation 30 mathematically presents a multiobjective optimization problem

$$\min(f_1(x), f_2(x), ..., f_k(x))$$
$$\text{s.t.} x \in X_1 \quad (30)$$

where K is the number of objectives and set X is the feasible set of decision vectors. The vector-valued objective function can be written as eq 31

$$f: X \to R^k, \ (f_1(x), f_2(x), ..., f_k(x))^T \quad (31)$$

MOGA was used via MATLAB-2020a. The following steps considered the reproductive procedure of the genetic algorithm: natural selection, crossover, mutation, fitness computation,

https://doi.org/10.1021/acsomega.1c04345
ACS Omega 2022, 7, 12493−12508

repair, updation of population, and elitism. While GA is related to one objective function, MOGA can consider more than one objective function. The upper and lower bounds were considered. The MOGA was run in MATLAB software. The pseudocode for the MOGA algorithm used in this study is shown in Figure 3.

4.2. WCA. The water cycle algorithm (WCA) mimics the flow of rivers and streams toward the sea based on the water cycle process. In the case of rain or precipitation, the primary population of design variables (i.e., the population of streams) is randomly increased following the raining process. The best individual variable (i.e., the best stream) with minimum cost function is the sea. Afterward, some good streams with cost function values close to the current best record are assumed as rivers, considering the other remaining streams to have flowed into rivers and the sea. The optimization algorithm should be started with a primary population representing a matrix of streams. For an N-dimensional optimization problem, the following algorithm can be developed using some equations.

$$N_{sr} = \text{number of Rivers} + 1 \tag{32}$$

$$N_{stream} = N_{pop} - N_{sr} \tag{33}$$

where N_{pop} and N represent the total population and the number of design variables, respectively.

$$NS_n = \text{round}\left(\left|\frac{\text{Cost}_n}{\sum_{i=1}^{N_{sr}} \text{Cost}_i}\right| \times N_{stream}\right), n = 1, 2, ..., N_{sr} \tag{34}$$

where NS_n is the number of streams that flow to the specific rivers and sea. The following equations may obtain the new position for streams and rivers.

$$\vec{X}_{Stream}^{i+1} = \vec{X}_{Stream}^{i} + \text{rand} \times C \times (\vec{X}_{River}^{i} - \vec{X}_{Stream}^{i}) \tag{35}$$

$$\vec{X}_{Stream}^{i+1} = \vec{X}_{Stream}^{i} + \text{rand} \times C \times (\vec{X}_{Sea}^{i} - \vec{X}_{Stream}^{i}) \tag{36}$$

$$\vec{X}_{River}^{i+1} = \vec{X}_{River}^{i} + \text{rand} \times C \times (\vec{X}_{Sea}^{i} - \vec{X}_{River}^{i}) \tag{37}$$

where rand is a uniformly distributed random numbers between 0 and 1. The new position of the streams is determined by

$$\vec{X}_{Stream}^{New} = \text{LB} + \text{rand} \times (\text{UB} - \text{LB}) \tag{38}$$

where LB and UB are lower and upper bounds defined by the given problem, respectively. The value of d_{max} adaptively decreases as follows

$$d_{max}^{i+1} = d_{max}^{i} - \frac{d_{max}^{i}}{\text{Max Iteration}} \tag{39}$$

```
Set the user parameter of the WCA: Npop, Ngr, dmar, and Maximum_Iteration.
Determine the number of streams (individuals) flowing toward the rivers and sea
using Eqs. (32) and (33).
• Create a random initial population.
• Define the intensity of flow (How many streams flow to their corresponding
rivers and sea) using Eq. (34)
        while (t < Maximum_Iteration) or (any stopping condition)
            for i = 1: Population Size (Npop)
            Stream flows to the corresponding rivers and sea using Eqs.(35) & (36)
            Calculate the objective function of the generated stream
              if F New_Stream <F_river
                River = New_Stream;
                 if F_New_Stream <F_Sea
                 Sea = New_Stream;
                 end if
              end if
            River flows to the sea using Eq. (37)
            Calculate the objective function of the generated river
                 if F_New_River <F_Sea
                   Sea = New_River;
                 end if
              end
            for i = 1: number of rivers (N)
            if (range (Sea and River) <dmar) or (rand <0.1)
            new streams are created using Eq. (38)
            Reduce the dmax using Eq. (39)
        end while
Postprocess results and visualization
```

Figure 4a shows a schematic view of a stream flowing toward a specific river along their connection line. Figure 4b shows the schematic of the WCA optimization process. Also, Figure 5 shows the flowchart of the water cycle algorithm.

4.3. Optimization Problem. The objective functions of the problem are as follows:

- Maximum production based on weight percentages
- Minimization of entropy generation

Two-objective optimization leads to a two-dimensional Pareto frontier. Thus, the closest solution in the population to the ideal point in the 2D space of the frontier would be considered as the optimum solution to the problem.

The preliminary community should be generated concerning some limitations in the input data, i.e., the constraints of the

https://doi.org/10.1021/acsomega.1c04345
ACS Omega 2022, 7, 12493−12508

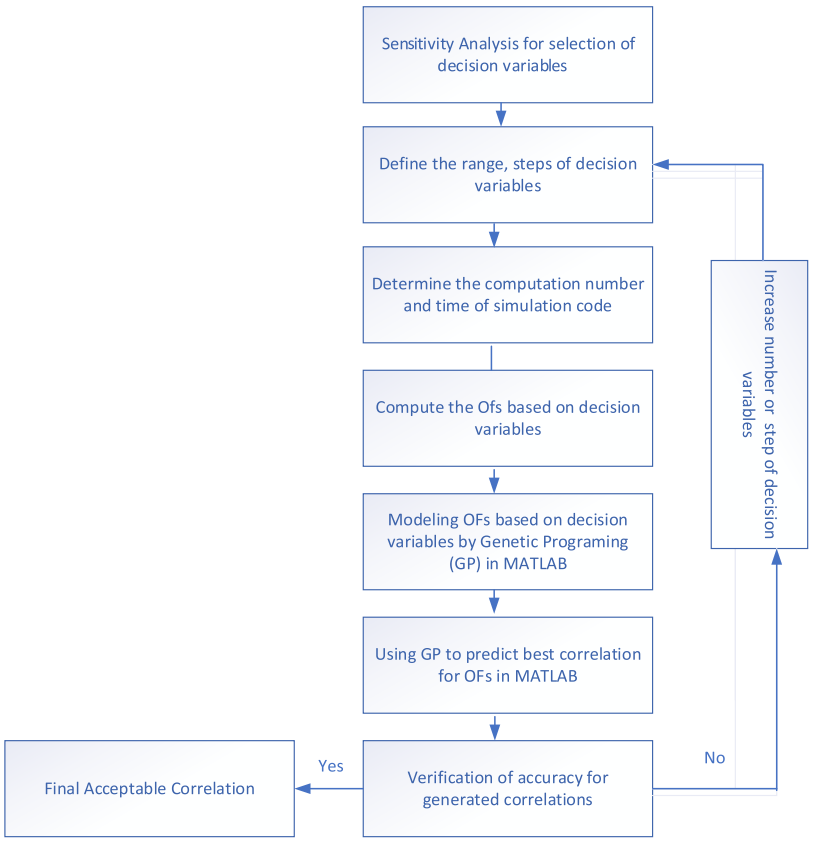

Figure 6. Algorithm using GP to generate OFs.

decision variables. The values of the constraints are shown in Table 3.

4.4. Genetic Programming. Genetic Programming (GP) generates prediction functions based on decision variables to reduce the optimization run time. In this regard, based on simulation results associated with varying decision variables, the best correlation for estimating objective functions have been proposed by the GP code. Figure 6 shows the algorithm of using GP to generate OFs.

5. RESULTS AND ANALYSIS

5.1. Results for the Reactor in the Reference State. In this research, the main objective was to produce ethylene. The main outputs of the propane thermal cracking reactor included ethylene, methane, propane, propylene, and hydrogen. To verify the computer code for modeling and simulation of the thermal cracking reactor, the simulation results were compared with an industrial case study.[28]

The percent of propane conversion and the weight of the products were derived by comparing with an industrial reactor.

Although coke production was neglected, according to Table 4, the simulation results match the practical results to a high degree of consistency. The weight percent of C_3H_6 had the highest inconsistency of 12%. The conversion percent difference falls to 0.01%, which was initially the main objective.

Figure 7 illustrates the outer wall temperature profile of the tube, derived from the temperature of the reactor surface in the industrial sample.[28]

Table 4 presents the results according to the temperature of the outer wall (Figure 8); Figure 8 also depicts the calculation of the governing equations and the temperature profile of the gas mixture. The temperature is 873.15 K at the starting point of the input. As heat is transferred along the tube, the chemical reactions progress, and the outer temperature reaches the wall temperature. Figure 9 depicts the reactor conversion percent, and Figure 10 depicts the weight percent profile of each product.

5.2. Generation of Correlation Using GP. Different simulations were performed to generate the prediction correlations for objective functions with the computer code in the range of decision variables. These data are transferred to the GP code, and the best prediction correlations for objective functions have been achieved, as shown in Table 5. When the mean square error (R^2) range is between 0.9 and 1, the accuracy is very high.

The verification of the following equations has been compared with the simulation data with high accuracy. These equations reduce the computation time by about 85%. Also, their accuracy is very high and acceptable.

5.3. Optimization Results. *5.3.1. Multiobjective Optimization.* Table 6 presents the Pareto Front optimum solutions for objective functions and decision variables based on MOGA. As shown, the optimum objective functions and corresponding decision variables were determined.

To draw the Pareto front and find the best solution that trade-off between multiple objectives, it is better first to rewrite the target functions in the Pareto optimal solutions so that the difference between the dimensions of the functions is neutralized in the concept of points distance from the ideal point. To make the answers dimensionless, we use the following relation

https://doi.org/10.1021/acsomega.1c04345
ACS Omega 2022, 7, 12493−12508

Table 4. Comparison of the Products of Simulated and Industrial Reactors

component	weight percent (wt %) of the simulated reactor	weight percent (wt %) of an industrial reactor[28]
conversion coefficient	90.61	90.60
CH_4	22.89	24.00
C_2H_4	36.82	34.50
C_3H_6	12.89	14.70
C_3H_8	9.38	9.30
H_2	1.67	1.20

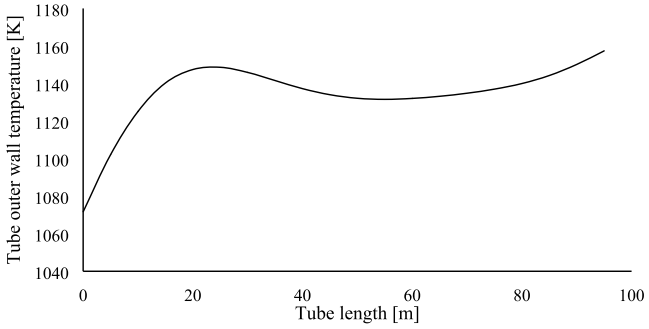

Figure 7. Temperature profile of the outer surface of the reactor with the industrial wall temperature.

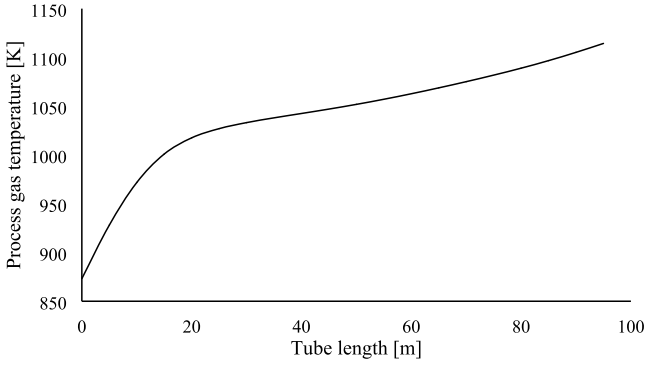

Figure 8. Temperature profile of the gas mixture in the reactor with industrial wall temperature.

$$OF_{DL,i,k} = \frac{OF_{i,k} - OF_{min,i}}{OF_{max,i} - OF_{min,i}} \quad (40)$$

$OF_{DL,i,k}$ is the dimensionless objective function for the i-M function and the kM response, i is the target function counter, and k is the response function in that target function. The presentation of the Pareto front for the dimensionless OFs is shown in Figure 11. The 2D normalized Pareto front indicates normalized entropy generation rate versus normalized products.

As shown in Figure 11, the point to the coordinates (1,0) is the equilibrium point or ideal point. From the Pareto front's optimal response set, any response closer to the ideal point is the optimal response. The concept of distance is used according to the following equation to find the closest answer to the ideal point

$$d_k = \sqrt{(OF_{1,k} - OF_{1,ideal})^2 + (OF_{2,k} - OF_{2,ideal})^2} \quad (41)$$

The minimum distance is calculated as 0.5913 and is related to the selected optimal solution, as shown in Table 5.

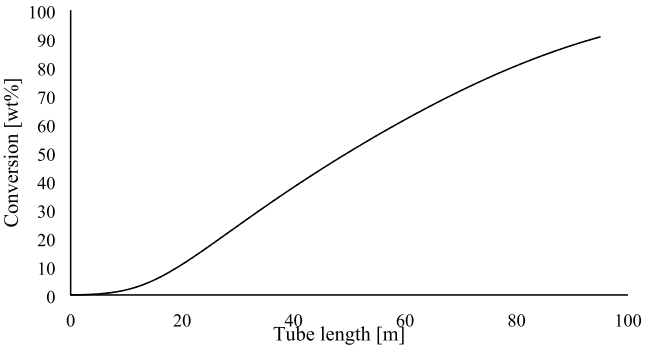

Figure 9. Conversion percent profile per unit length of the reactor with industrial wall temperature.

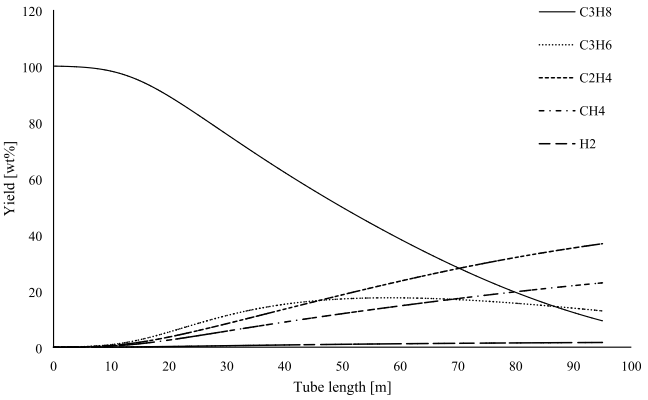

Figure 10. Weight percent of the products along the reactor with industrial wall temperature.

The optimum values of OFs and decision variables based on MOGA are determined and shown in Table 7. The weight percentage of the basic system products is 60.615%, and the entropy production rate is 1048 J/s. The table above shows that the weighted percentage of products and the system's entropy production rate after optimization reached 61.13% and 899.8 J/s, displaying an improvement of 0.85 and 16.51%, respectively. The GP and non-GP results also showed similar improvements. However, the computation time of the GP declined significantly (about 85% of the base case).

With MOWCA, the Pareto front optimum solution and its decision variables are indicated in Table 8.

The Pareto front optimal solution based on MOWCA is demonstrated in Figure 12.

The weight percentage of the products produced in the basic system is 60.61%, and the entropy production rate is 1048 J/s. As shown in Table 9, the weighted percentage of products and the entropy production rate of the system after optimization reached 61.81% and 882.72 J/s, respectively, which resulted in an improvement of 1.97 and 18.77%, respectively. As shown in Table 9, the optimization with GP and non-GP algorithms shows similar results.

5.3.2. Single-Objective Optimization. In this case, two optimization processes are implemented with one of the target functions. Optimization results to maximize product production lead to 64.36% by weight of system products, equivalent to a 6.17% increase in product production. The single-objective optimization response aims to maximize product production, as shown in Table 10.

https://doi.org/10.1021/acsomega.1c04345
ACS Omega 2022, 7, 12493−12508

Table 5. Objective Function Correlation Generated by GP

objective function	best equation	mean square error (R^2)
products (%)	$0.00127 \times P_{gas_{in}} + 7045.399 \times \log(T_w) + 1.55E{-}28 \times P_{gas_{in}} \times T_w^{\,8} - 42402.84 - 6.23 \times T_w - 1.38E - 9 \times P_{gas_{in}} \times T_w^{\,2}$	0.97
entropy generation	$123.876 + 0.00189717 \times P_{gas_{in}} - \frac{4.42E12}{T_{gas_{in}} \times P_{gas_{in}}} + \frac{3.78E5 + 371.07 \times ma}{T_{gas_{in}}} + 1.498 \times \frac{T_w}{T_{gas_{in}} \times P_{gas_{in}}^{\,2}} - 1.60E17 \times \frac{T_w^{\,2}}{T_{gas_{in}} \times P_{gas_{in}}^{\,3}}$	0.94

Table 6. Pareto front optimum solutions for Objective Functions Based on MOGA

OF1 products (%)	OF2 entropy (J/K s)	DV1 T_{gas_in} (K)	DV2 P_{gas_in} (kPa)	DV3 m_a (g/s)	DV4 $T_{w,in}$ (K)
44.19	699.63	852.71	250.002	750.00	1000.00
44.19	699.63	852.71	250.002	750.00	1000.00
48.41	741.06	853.11	250.003	750.76	1010.39
64.45	986.14	852.79	250.004	751.05	1098.55
54.50	807.46	852.88	250.004	750.30	1028.80
56.42	831.17	853.15	250.004	750.40	1035.97
55.44	818.78	852.99	250.003	750.22	1032.20
46.07	717.76	852.91	250.003	750.53	1004.44
52.80	787.75	852.97	250.003	750.25	1023.12
64.17	971.10	853.49	250.005	750.43	1090.57
60.10	882.90	853.03	250.004	750.45	1053.11
61.61	908.49	852.94	250.004	750.22	1062.63
51.84	777.23	853.31	250.004	750.73	1020.13
57.14	840.46	853.07	250.004	750.43	1038.88
63.39	946.53	853.34	250.004	750.45	1078.57
45.68	713.97	852.83	250.003	750.39	1003.51
63.15	940.32	853.40	250.005	750.39	1075.81
46.94	726.23	853.01	250.003	750.42	1006.60
61.29	902.59	853.46	250.004	750.32	1060.42
57.84	849.82	853.28	250.003	750.53	1041.89
58.72	862.21	852.95	250.002	750.40	1045.97
63.64	953.19	853.46	250.004	750.35	1081.70
62.87	933.99	853.27	250.002	750.60	1073.00
53.02	790.38	852.96	250.004	750.40	1023.85
59.33	871.11	852.94	250.004	750.44	1048.98
64.04	966.05	853.28	250.004	750.43	1087.93
64.56	1001.43	853.54	250.005	751.93	1108.04
52.43	783.61	852.97	250.004	750.22	1021.96
49.20	748.99	852.76	250.003	750.16	1012.52
45.08	708.22	853.06	250.003	750.46	1002.08
53.46	795.40	852.93	250.003	750.42	1025.28
61.13	899.80	853.42	250.004	750.36	1059.36
46.98	726.65	852.95	250.003	750.40	1006.71
44.44	701.94	852.72	250.002	750.02	1000.56
60.60	891.09	852.76	250.004	750.39	1056.04
50.23	759.82	853.21	250.003	750.57	1015.38
58.08	853.21	853.17	250.004	750.41	1043.00
64.25	974.33	853.52	250.004	750.42	1092.29
60.58	890.60	853.27	250.004	750.43	1055.92
54.33	805.38	853.09	250.004	750.24	1028.21
54.96	813.05	853.28	250.004	750.62	1030.44
55.77	823.00	852.72	250.004	750.20	1033.46
61.95	914.86	853.22	250.004	750.54	1065.11
62.68	929.68	852.97	250.004	750.37	1071.16
56.08	826.87	853.29	250.003	750.68	1034.62
64.55	996.99	853.48	250.005	751.88	1105.13
47.57	732.49	852.80	250.003	750.27	1008.21
62.39	923.42	853.46	250.005	750.37	1068.63

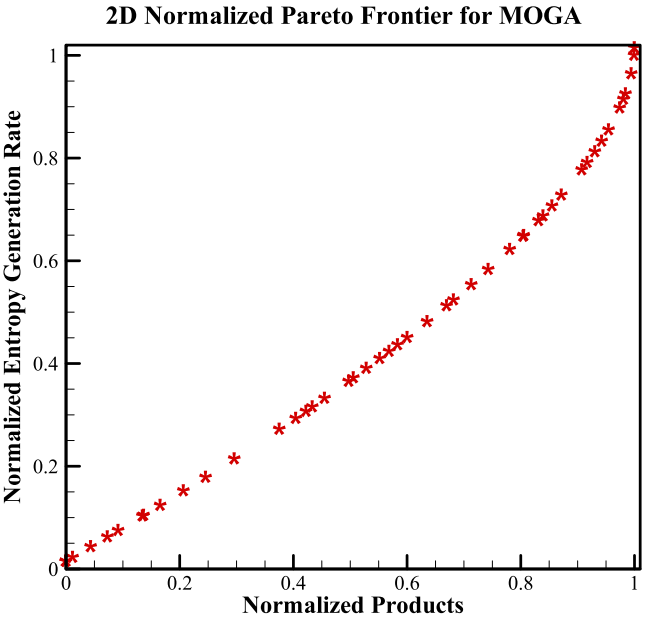

Figure 11. Normalized Pareto front optimum solution obtained with MOGA.

Table 7. Pareto Front Optimum Solutions for Objective Functions Based on MOGA

optimum objective function parameters	with GP value	without GP value
products (normalized)	0.83	0.83
entropy generation (normalized)	0.66	0.66
products (%)	61.13	61.13
entropy generation (J/K s)	899.80	899.80
optimum decision variable parameters	with GP value	without GP value
T_{gas_in} (K)	853.42	853.42
P_{gas_in} (bar)	25	25
m_a (g/s)	750.36	750.36
T_{w_in} (K)	1059.36	1059.36

The optimization results aimed at minimizing the entropy production rate lead to the production of 687.99 (J/K s) entropy in the system, equivalent to a decrease of 52.38% in the production of the entropy production rate of the system. The solution to the single-objective optimization to minimize the entropy production of the system is indicated in Table 11.

Also, a single optimization using WCA has been performed. The optimization results aim to maximize the product, leading to the formation of 64.56% by weight of system products, equivalent to a 6.51% increase in product production as determined in Table 12.

The optimization results aimed at minimizing the entropy production rate lead to the production of 687.50 (J/K s) entropy

https://doi.org/10.1021/acsomega.1c04345
ACS Omega 2022, 7, 12493−12508

Table 8. Pareto Front Optimum Solutions for Objective Functions Based on MOWCA

OF1	OF2	DV1	DV2	DV3	DV4
products (%)	entropy (J/K s)	T_{gas_in} (K)	P_{gas_in} (kPa)	m_a (g/s)	T_{w_in} (K)
64.56	962.27	943.15	250.000	750.00	1108.01
44.19	689.91	943.15	250.000	750.00	1000.00
44.19	689.91	895.34	309.530	816.06	1119.54
64.56	962.27	943.15	250.000	750.00	1108.01
63.37	912.68	943.15	250.000	750.00	1078.33
62.08	886.71	943.15	250.000	750.00	1066.12
48.95	733.39	943.15	250.000	753.29	1011.83
45.71	702.98	943.15	250.000	750.00	1003.58
44.78	694.93	943.15	250.000	750.00	1001.36
63.97	928.76	943.15	250.000	750.73	1086.63
48.07	724.02	932.18	384.524	766.49	1100.51
56.53	812.96	943.15	250.422	750.90	1036.40
50.27	749.95	913.24	250.067	750.66	1015.50
57.37	820.33	907.80	285.339	837.65	1050.34
50.96	756.77	943.15	250.000	763.98	1017.51
64.42	946.32	943.15	250.000	750.00	1097.14
46.03	705.98	943.15	250.016	750.30	1004.36
55.95	806.38	943.15	250.435	750.93	1034.14
46.73	712.18	926.17	253.355	776.41	1028.38
52.59	770.42	943.15	250.504	751.07	1022.44
49.77	744.57	912.72	250.000	750.20	1014.08
54.50	787.35	943.15	250.000	750.00	1028.82
55.38	799.93	943.15	250.448	750.95	1031.97
58.30	832.55	871.60	272.639	757.16	1116.20
49.51	737.11	901.89	341.795	836.10	1132.17
55.05	793.36	943.15	250.000	750.00	1030.79
60.70	864.94	943.15	250.000	751.46	1056.65
57.87	825.99	869.25	306.906	819.11	1194.70
54.02	782.21	881.20	310.435	779.45	1051.96
63.59	921.19	934.42	250.020	750.20	1081.01
58.87	838.76	908.91	424.713	779.49	1054.57
53.15	777.29	943.15	250.000	760.60	1024.25
47.77	721.33	943.15	250.000	750.00	1008.73
52.18	764.33	926.52	413.089	782.40	1092.34
59.53	850.37	943.15	250.341	750.73	1050.06
47.30	717.09	943.15	250.000	750.00	1007.52
59.23	843.62	873.70	280.983	805.55	1158.11
61.21	872.22	943.15	250.000	750.00	1059.89
60.19	859.58	943.15	250.000	756.88	1053.65
61.81	882.72	943.15	250.000	751.65	1064.08
64.45	951.98	923.33	312.665	824.69	1118.13
51.61	758.82	943.15	250.000	753.03	1019.44
61.43	875.80	907.61	353.490	820.16	1009.01
53.40	779.90	943.15	250.000	760.50	1025.09
44.50	692.64	943.15	250.010	750.15	1000.71
60.02	854.45	943.15	250.000	750.00	1052.70
47.04	714.72	943.15	250.000	750.00	1006.85
51.85	761.11	859.39	334.392	836.31	1131.28

in the system, equivalent to a decrease of 52.49% in the production of the entropy production rate of the system, as shown in Table 13.

5.4. Computational Time. The computational time for MOGA, MOWCA, GP-MOGA, and GP-MOWCA are indicated in Table 14. In the GP-MOGA and GP-MOWCA, the time for generation of data sets and GP correlations have been considered.

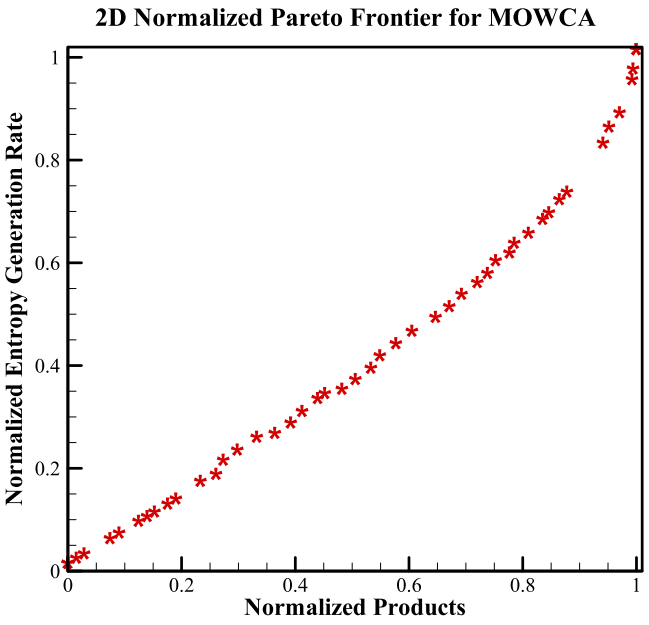

Figure 12. Normalized Pareto front optimum solution obtained with MOWCA.

Table 9. Pareto Front Optimum Solutions for Objective Functions Based on MOWCA

optimum objective function parameters	with GP value	without GP value
products (normalized)	0.86	0.86
entropy generation (normalized)	0.71	0.71
products (%)	61.81	61.81
entropy generation (J/K s)	882.72	882.72
optimum decision variable parameters	with GP value	without GP value
$T_{gas,in}$ (K)	943.15	943.15
$P_{gas,in}$ (bar)	25	25
m_a (g/s)	751.65	751.65
$T_{w,in}$ (K)	1064.08	1064.08

Table 10. Results of Maximization of the Product by GA

optimum objective function parameters	with GP value	without GP value
products (%)	64.36	64.36
entropy generation (J/K s)	1022.20	1022.20
optimum decision variable parameters	with GP value	without GP value
$T_{gas,in}$ (K)	908.35	908.35
$P_{gas,in}$ (bar)	25.29	25.29
m_a (g/s)	785.71	785.71
$T_{w,in}$ (K)	1107.42	1107.42

Table 11. Results of Minimization of Entropy Generation by GA

optimum objective function parameters	with GP value	without GP value
products (%)	48.92	48.92
entropy generation (J/K s)	688.00	688.00
optimum decision variable parameters	with GP value	without GP value
T_{gas_in} (K)	845.85	845.85
P_{gas_in} (bar)	35.39	35.39
m_a (g/s)	750.27	750.27
T_{w_in} (K)	1000.00	1000.00

The computation time is based on Intel Core i7-8750H with 6 CPU cores and 16 GB memory. As seen, the computation time is

https://doi.org/10.1021/acsomega.1c04345
ACS Omega 2022, 7, 12493−12508

Table 12. Results of Maximization of the Product by WCA

optimum objective function parameters	with GP value	without GP value
products (%)	64.56	64.56
entropy generation (J/K s)	1009.20	1009.20
optimum decision variable parameters	with GP value	without GP value
T_{gas_in} (K)	915.27	915.27
P_{gas_in} (bar)	35.39	35.39
m_a (g/s)	25	25
T_{w_in} (K)	1108.01	1108.01

Table 13. Results of Minimization of Entropy Generation by WCA

optimum objective function parameters	with GP value	without GP value
products (%)	59.66	59.66
entropy generation (J/K s)	687.50	687.50
optimum decision variables parameters	with GP value	without GP value
T_{gas_in} (K)	878.08	878.08
P_{gas_in} (bar)	28.03	28.03
m_a (g/s)	799.67	799.67
T_{w_in} (K)	1161.73	1161.73

Table 14. Comparison of Computation time for MOGA, MOWCA, GP-MOGA, and GP-MOWCA

methodology	MOGA	MOWCA	GP-MOGA	GP-MOWCA
computation time (s)	63 056.8	61 753	34 270	33 380
computation time (h)	17.51	17.15	9.52	9.27

reduced significantly in GP-MOWCA and GP-MOGA compared with MOGA and MOWCA.[40]

6. CONCLUSIONS

A thermal cracking reactor was investigated in this study. The input feed was propane and water steam, and the main output products were propane, methane, ethylene, propylene, and hydrogen. The amount of entropy generated by the sources and the governing equations was investigated.

Single-objective and two-objective optimizations using GA and WCA were performed to maximize products and minimize entropy generation. Decision variables were the inlet gas temperature, inlet gas pressure, the mass flow rate of the inlet air, and the wall. GP was employed to generate the best correlations to predict objective functions based on key variables to reduce the run time of optimization runs.

Based on single-objective optimization, the following results were obtained:

- Maximizing product production using GA and WCA led to 64.36 and 64.56% by weight of system products equivalent to a 6.17 and 6.51% increase in the product compared to the base case.
- Minimizing the entropy production rate using the GA and WCA led to a decrease of 52.38 and 52.49% compared to the base case in the entropy generation rate of the system.

Based on two-objective optimization, the following results were obtained:

- The weighted percentage of products and the entropy production rate improved 0.85% and 16.51% compared with the base case using the MOGA algorithm, and 1.97 and 18.77% compared to the base case.

It is suggested that future studies will address exergonic and exergoeconomic parameters. For studies on the optimization problem, environmental impacts are critical factors that should be further investigated.

AUTHOR INFORMATION

Corresponding Author

Gholamreza Salehi − *Department of Mechanical Engineering, Central Tehran Branch, Islamic Azad University, Tehran 11936-53471, Iran;* orcid.org/0000-0002-7866-358X; Phone: +989122031671; Email: gh.salehi@iauctb.ac.ir

Authors

Peyman Roudgar Saffari − *Department of Mechanical Engineering, Adiban Institute of Higher Education, Garmsar 35819-69855, Iran;* orcid.org/0000-0002-8419-8602

Hesamoddin Salarian − *Department of Mechanical Engineering, Nour Branch, Islamic Azad University, Nour 15858-54289, Iran*

Ali lohrasbi − *Department of Mechanical Engineering, Islamic Azad University of Nowshahr Branch, Nowshahr 46517-39948, Iran*

Mohammad Hasan Khoshgoftar Manesh − *Energy, Environmental and Biological Systems Research Lab (EEBRlab), Division of Thermal Sciences and Energy Systems, Department of Mechanical Engineering, Faculty of Technology & Engineering, University of Qom, Qom 37137-44003, Iran*

Complete contact information is available at: https://pubs.acs.org/10.1021/acsomega.1c04345

Notes

The authors declare no competing financial interest.

NOMENCLATURE

j	jth component
dz	the length dz
F_j	the intensity of the molar flow of the jth component
α_{ij}	stoichiometric coefficient of the jth component in the ith reaction
R_j	overall velocity of the production and/or consumption of the jth component
r_i	the velocity of the ith reaction
K_i	the specific velocity of the ith reaction
c_j	the molar concentration of the jth component
y_j	molar ratio
ΔH_i	the heat of the ith reaction
$J_q(z)$	heat flux transferred from the outer heat source to the reaction flow in the location z of the reactor
C_{pj}	heat capacity of the jth component
α	unit conversion factor
ρ	gas density
u	gas speed
M_m	gas mixture molecular weight
Λ	the angle of the bends, which is equal to 180°
T_w	surface temperature
T_∞	fluid temperature
h	the coefficient of the convection heat transfer
T_c	the temperature of the tube center
T_b	bulk temperature
T_{bo}	outlet bulk temperature
S_{in}	entropy of the inlet flow
S_{out}	entropy of the outlet flow
ΔS_u	entropy induced by heat transfer

https://doi.org/10.1021/acsomega.1c04345
ACS Omega 2022, 7, 12493−12508

σ locally generated entropy
A coefficient of exponential function or coefficient of frequency
E the activation energy (expressed in J/mol or cal/mol)
R ideal gas constant
T absolute temperature, K

REFERENCES

(1) Zhou, S.; Chen, L.; Sun, F. Constructal Optimization for a Solid-Gas Reactor Based on Triangular Element. *Sci. China, Ser. E* **2008**, *51*, 1554−1562.
(2) Gao, G.-Y.; Wang, M.; Pantelides, C. C.; Li, X.-G.; Yeung, H. Mathematical Modeling and Optimal Operation of Industrial Tubular Reactor for Naphtha Cracking. *Comput.-Aided Chem. Eng.* **2009**, *27*, 501−506.
(3) Masoumi, M.; Shahrokhi, M.; Sadrameli, M.; Towfighi, J. Modeling and Control of a Naphtha Thermal Cracking Pilot Plant. *Ind. Eng. Chem. Res.* **2006**, *45*, 3574−3582.
(4) Ghasemi, H. M.; Gilani, N.; Daryan, J. T. CFD Simulation of Propane Thermal Cracking Furnace and Reactor: A Case Study. *Int. J. Chem. React. Eng.* 2016, *15*. DOI: 10.1515/ijcre-2016-0125.
(5) Ghashghaee, M.; Karimzadeh, R. Dynamic Modeling and Simulation of Steam Cracking Furnaces. *Chem. Eng. Technol.* **2007**, *30*, 835−843.
(6) Zheng, S.; Zhang, X.; Qi, C.; Zhou, H. Modeling of Heat Transfer and Pyrolysis Reactions in Ethylene Cracking Furnace Based on 3-D Combustion Monitoring. *Int. J. Therm. Sci.* **2015**, *94*, 28−36.
(7) Barazandeh, K.; Dehghani, O.; Hamidi, M.; Aryafard, E.; Rahimpour, M. R. Investigation of Coil Outlet Temperature Effect on the Performance of Naphtha Cracking Furnace. *Chem. Eng. Res. Des.* **2015**, *94*, 307−316.
(8) Nummedal, L.; Kjelstrup, S. Equipartition of Forces as a Lower Bound on the Entropy Production in Heat Exchange. *Int. J. Heat Mass Transfer* **2001**, *44*, 2827−2833.
(9) Sauar, E.; Nummedal, L.; Kjelstrup, S. The Principle of Equipartition of Forces in Chemical Reactor Design: The Ammonia Synthesis. *Comput. Chem. Eng.* **1999**, *23*, S499−S502.
(10) Kjelstrup, S.; Island, T. V. The Driving Force Distribution for Minimum Lost Work in a Chemical Reactor Close to and Far from Equilibrium. 2. Oxidation of SO2. *Ind. Eng. Chem. Res.* **1999**, *38*, 3051−3055.
(11) de Koeijer, G. M.; Kjelstrup, S.; Salamon, P.; Siragusa, G.; Schaller, M.; Hoffmann, K. H. Comparison of Entropy Production Rate Minimization Methods for Binary Diabatic Distillation. *Ind. Eng. Chem. Res.* **2002**, *41*, 5826−5834.
(12) de Koeijer, G.; Røsjorde, A.; Kjelstrup, S. Distribution of Heat Exchange in Optimum Diabatic Distillation Columns. *Energy* **2004**, *29*, 2425−2440.
(13) Nummedal, L.; Kjelstrup, S.; Costea, M. Minimizing the Entropy Production Rate of an Exothermic Reactor with a Constant Heat-Transfer Coefficient: The Ammonia Reaction. *Ind. Eng. Chem. Res.* **2003**, *42*, 1044−1056.
(14) Røsjorde, A.; Kjelstrup, S. The Second Law Optimal State of a Diabatic Binary Tray Distillation Column. *Chem. Eng. Sci.* **2005**, *60*, 1199−1210.
(15) Wilhelmsen, Ø.; Johannessen, E.; Kjelstrup, S. Energy Efficient Reactor Design Simplified by Second Law Analysis. *Int. J. Hydrogen Energy* **2010**, *35*, 13219−13231.
(16) Johannessen, E.; Kjelstrup, S. Minimum Entropy Production Rate in Plug Flow Reactors: An Optimal Control Problem Solved for SO2 Oxidation. *Energy* **2004**, *29*, 2403−2423.
(17) Kingston, D.; Razzitte, A. C. Entropy Production in Chemical Reactors. *J. Non-Equilib. Thermodyn.* **2017**, *42*, 265−275.
(18) Chen, L.; Zhang, L.; Xia, S.; Sun, F. Entropy Generation Minimization for CO 2 Hydrogenation to Light Olefins. *Energy* **2018**, *147*, 187−196.
(19) Røsjorde, A.; Kjelstrup, S.; Johannessen, E.; Hansen, R. Minimizing the Entropy Production in a Chemical Process for Dehydrogenation of Propane. *Energy* **2007**, *32*, 335−343.
(20) Abdous, M. A.; Saffari, H.; Avval, H. B.; Khoshzat, M. Investigation of Entropy Generation in a Helically Coiled Tube in Flow Boiling Condition under a Constant Heat Flux. *Int. J. Refrig.* **2015**, *60*, 217−233.
(21) Kurnia, J. C.; Sasmito, A. P.; Shamim, T.; Mujumdar, A. S. Numerical Investigation of Heat Transfer and Entropy Generation of Laminar Flow in Helical Tubes with Various Cross Sections. *Appl. Therm. Eng.* **2016**, *102*, 849−860.
(22) Vandewalle, L. A.; Van Cauwenberge, D. J.; Dedeyne, J. N.; Van Geem, K. M.; Marin, G. B. Dynamic Simulation of Fouling in Steam Cracking Reactors Using CFD. *Chem. Eng. J.* **2017**, *329*, 77−87.
(23) Mu, P.; Gu, X. Thermal Cracking Furnace Optimal Modeling Based on Enriched Kumar Model by Free-Radical Reactions. *Processes.* **2020**, *8*, No. 91.
(24) Zhou, L.; Li, K.; Hang, P.; Liu, G. Optimization of the Ethane Thermal Cracking Furnace Based on the Integration of Reaction Network. *Clean Technol. Environ. Policy* **2021**, *23*, 879−887.
(25) Narasimharao, K.; Alshehri, A. Gold Supported Yttrium Oxide Nanorods for Catalytic Oxidative Cracking of N-Propane to Light Olefins. *Fuel* **2020**, *278*, No. 118375.
(26) Ebrahimian, S.; Iranshahi, D.; Bahmanpour, A. M. A Novel Reactor Concept for Thermal Integration of Naphtha Reforming with Propane Ammoxidation. *Chem. Eng. Process. Process Intensif.* **2019**, *146*, No. 107659.
(27) Barnoon, P.; Toghraie, D.; Mehmandoust, B.; Fazilati, M. A.; Eftekhari, S. A. Comprehensive Study on Hydrogen Production via Propane Steam Reforming inside a Reactor. *Energy Rep.* **2021**, *7*, 929−941.
(28) Berreni, M.; Wang, M. Modelling and Dynamic Optimization of Thermal Cracking of Propane for Ethylene Manufacturing. *Comput. Chem. Eng.* **2011**, *35*, 2876−2885.
(29) Rezaeimanesh, M.; Asghar Ghoreyshi, A.; Peyghambarzadeh, S. M.; Hassan Hashemabadi, S. A Coupled CFD Simulation Approach for Investigating the Pyrolysis Process in Industrial Naphtha Thermal Cracking Furnaces. *Chin. J. Chem. Eng.* **2021**, DOI: 10.1016/j.cjche.2021.03.028.
(30) Bi, K.; Zhang, S.; Zhang, C.; Li, H.; Huang, X.; Liu, H.; Qiu, T. Knowledge Expression, Numerical Modeling and Optimization Application of Ethylene Thermal Cracking: From the Perspective of Intelligent Manufacturing. *Chin. J. Chem. Eng.* **2021**, *38*, 1−17.
(31) Yuan, B.; Zhang, Y.; Du, W.; Wang, M.; Qian, F. Assessment of Energy Saving Potential of an Industrial Ethylene Cracking Furnace Using Advanced Exergy Analysis. *Appl. Energy* **2019**, *254*, No. 113583.
(32) Rebordinos, J. G.; Herce, C.; González-Espinosa, A.; Gil, M.; Cortés, C.; Brunet, F.; Ferré, L.; Arias, A. Evaluation of Retrofitting of an Industrial Steam Cracking Furnace by Means of CFD Simulations. *Appl. Therm. Eng.* **2019**, *162*, No. 114206.
(33) Meng, D.; Shao, C.; Zhu, L. Two-Level Comprehensive Energy-Efficiency Quantitative Diagnosis Scheme for Ethylene-Cracking Furnace with Multi-Working-Condition of Fault and Exception Operation. *Energy* **2022**, *239*, No. 121835.
(34) Saffari, P. R.; Salarian, H.; lohrasbi, A.; Salehi, G. Entropy Generation Analysis of a Thermal Cracking Reactor. *ACS Omega* **2021**, *6*, 6335−6347.
(35) Meyers, R. A.; Meyers, R. A. *Handbook of Petrochemicals Production Processes*; McGraw-Hill, 2005.
(36) Froment, G. F.; Bischoff, K. B.; De Wilde, J. *Chemical Reactor Analysis and Design*; Wiley: New York, 1990; Vol. 2.
(37) Sundaram, K. M.; Froment, G. F. Modeling of Thermal Cracking Kinetics—I: Thermal Cracking of Ethane, Propane and Their Mixtures. *Chem. Eng. Sci.* **1977**, *32*, 601−608.
(38) Shamshirband, S.; Khoshnevisan, B.; Yousefi, M.; Bolandnazar, E.; Anuar, N. B.; Abdul Wahab, A. W.; Khan, S. U. R. A Multi-Objective Evolutionary Algorithm for Energy Management of Agricultural Systems—A Case Study in Iran. *Renewable Sustainable Energy Rev.* **2015**, *44*, 457−465.

https://doi.org/10.1021/acsomega.1c04345
ACS Omega 2022, 7, 12493−12508

(39) Eskandar, H.; Sadollah, A.; Bahreininejad, A.; Hamdi, M. Water Cycle Algorithm – A Novel Metaheuristic Optimization Method for Solving Constrained Engineering Optimization Problems. *Comput. Struct.* **2012**, *110–111*, 151–166.
(40) Ghosh, P. K.; Sadhu, P. K.; Basak, R.; Sanyal, A. Energy Efficient Design of Three Phase Induction Motor by Water Cycle Algorithm. *Ain Shams Eng. J.* **2020**, *11*, 1139–1147.

https://doi.org/10.1021/acsomega.1c04345
ACS Omega 2022, 7, 12493–12508

https://doi.org/10.1021/acsomega.1c04345
ACS Omega 2022, 7, 12493−12508